Structural Analysis of some Alkaline-earth-metal–Copper Oxide Catalysts for Hydrocarbon Oxidation or NO Decomposition

Lucio Forni,* Cesare Oliva and Francesco P. Vatti
Dip. Chimica Fisica ed Elettrochimica, Universita' di Milano, Via C. Golgi 19, I-20133 Milano, Italy
Nataliya A. Sinitsina, Serghej V. Sorochkin, Alexandr V. Moev and Anatolij V. Vishniakov
Mendeleev Institute of Chemical Technology, Myusskaja Sq. 9, Moscow, USSR

Some Ca–Cu–O, Sr–Cu–O and Ca–Sr–Cu–O defective perovskite-like mixtures have been prepared by the sol–gel technique and tested by means of a pulse reactor as possible catalysts for the title reactions. The characterisation of these preparations by several techniques, such as X-ray diffraction (XRD), scanning electron microscopy–electron probe microanalysis (SEM–EPMA), temperature-programmed desorption–temperature-programmed reaction–mass spectrometry (TPD–TPR–MS), electron paramagnetic resonance spectroscopy (EPR) and sorption–desorption of nitrogen, showed that the catalytic activity for both the reactions appears to be connected with the presence of a layer-like crystal structure approximating a two-dimensional antiferromagnet, stable within a sufficiently wide range of temperature. When oxygen, either added during the oxidation reaction or forming after the decomposition of NO, bridges together neighbouring Cu^{2+} ions not previously linked to oxygen, strongly interacting dipole systems form.

It has been known for a long time that transition-metal oxides can catalyse the partial oxidation or ammoxidation of alkenic or alkylaromatic hydrocarbons to aldehydes or nitriles. Among them CuO can catalyse the oxidation of propene to acrolein, although the short durability of the catalyst makes it practically useless for application purposes. One interpretation of such behaviour was based on the lack of isolated sites on the solid surface with metal–oxygen bonds of the required strength.[1] To improve the durability of CuO as a mild oxidation catalyst, attempts have been made to promote it by adding other oxides, so permitting variations of the oxygen content of the active phase, at least within definite limits. This has been extensively studied on the superconducting YBCO (yttrium, barium, copper oxide) mixtures.[2,3] For instance, it has been found that the catalytic behaviour of the $YBa_2Cu_3O_{7-x}$ phase strongly depends on the value of x, since a transition from orthorhombic to tetragonal structure takes place on varying x from 7 to 6.4.[4] This affects the superconducting properties of the material, as well as its catalytic activity towards the oxidation of methanol to formaldehyde.[5] Several other reactions have been studied recently on similar oxide mixtures, among which the selective ammoxidation of toluene to benzonitrile[6,7] and the decomposition of NO[8] can be cited.

The superconducting properties of YBCO materials seem to be connected with the presence of Cu^{3+} species in the solid, while the particular feature characterising copper oxide as a solid catalyst usually relies on the ability of the Cu^{2+} ion to be reduced to Cu^+, which in turn is promptly reoxidised to Cu^{2+}. The characteristic behaviour of YBCO catalysts has been explained as due to the presence of structurally isolated Cu layers in which easily removable oxygen is present.[9] After removal of the latter, layers of Cu^+ ions form, which are able to adsorb oxygen[10] giving rise to the nucleophilic oxygen species involved in selective oxidation.[11,12]

The Cu^+ ion is by far less stable than Cu^{2+} in copper oxide. However, it may be stabilised by inserting it in a relatively stable crystalline oxide phase in which some other cation is present. The ability of such a host phase to accommodate the Cu^+ guest ions in the oxide framework structure depends both on the specific electric charge and on the radii of both host and guest ions. The more similar are these parameters, the better the guest ions can be accommodated within the crystalline framework structure. In the case of the YBCO structure, the stabilisation of Cu^+ species is particularly favoured, since the Y^{2+} ionic radius (0.93 Å) is very close to that of Cu^+ (0.96 Å).

However, a similar role could be played in these perovskite-like structures by both Ca^{2+} and Sr^{2+}, the ionic radii of which are 0.99 and 1.13 Å, respectively. Hence, the goal of the present work was to prepare Ca–Cu–O, Sr–Cu–O and Ca–Sr–Cu–O mixtures to be tested as possible catalysts for the mild oxidation of toluene to benzaldehyde or for the decomposition of NO, and to characterise them quite extensively by various techniques.

Experimental

Catalysts

Four oxide mixtures [$SrCuO_{2+\delta}$, $Sr_3Cu_5O_{8+\delta}$, $Ca_2CuO_{3+\delta}$ and $(Ca_{0.55}Sr_{0.45})_3Cu_5O_{8+\delta}$, referred to as 1_v–4_v and 1_a–4_a, respectively, the subscripts v and a meaning calcination *in vacuo* or in air, respectively] were prepared, by thoroughly mixing at 343–363 K a 30 wt.% aqueous polyacrylic acid (PAA) solution and aqueous nitrate solutions. The molar ratio between PAA (*ca.* 4000 MW) and the nitrates was >50. A gel was obtained, which was dried (473–523 K) overnight and precalcined in air at 773–973 K. A final 50 h heat treatment followed. Two different conditions were chosen for this treatment, namely calcination *in vacuo* (*ca.* 100 Pa oxygen partial pressure) or in air. In any case, the calcination temperature was 1143 K. The chemical analysis (iodometric titration) showed a deviation from the stoichiometric oxygen index of 0.1, 0.15, 0.01 and 0.4, for the 1_a–4_a samples, respectively. For the sake of simplicity, in the following the samples will be referred to either by their symbols (1_v, *etc.*) or by the stoichiometric formula, *i.e.* by neglecting the value of δ.

The choice of a high-temperature final treatment was considered particularly suitable not only for ensuring the formation of a thermally stable perovskite-like solid solution, but also for the use of these solids as catalysts for the previously cited reactions. Indeed, partial oxidation usually requires low-surface area catalysts, in order to make the contact time of the reactant gas with the catalyst as short as possible, so reducing the risk of complete oxidation to CO_2 and H_2O end-products. On the other hand, the decomposition of NO usually takes place directly in the flue gas from the burners of power stations. Hence the catalyst must withstand possible temperature fluctuations.

Several techniques were employed for characterising the catalysts. The presence or absence of known crystalline phases was checked by XRD (Debye method, Cu-Kα radiation, Ni filtered) on a Siemens D-500 instrument. The patterns were compared with literature data.[13] The morphology of the solids was analysed by SEM at various magnifications on a Cambridge Stereoscan 150 microscope. The surface concentration of the various cations was checked by EPMA on a Link Mod. 860 apparatus, by integrating the counts for a preset lifetime and for a large number of different positions over the sample at various magnifications, *i.e.* by including either single crystals, or a reasonably large number of different crystals. BET surface area and porosity were measured by sorption–desorption of nitrogen at the liquid-nitrogen temperature by means of a Sorptomatic 1800 C. Erba instrument. Sorption–desorption behaviour and catalytic activity were tested by means of a previously described TPD–TPR apparatus[14] equipped with a UTI-100 quadrupolar mass spectrometer as a detecting unit and employing helium as carrier gas. The presence of adsorbed radicals, as well as the nature of the Cu-based paramagnetic sites, was analysed by EPR on a Varian E-line Century Series apparatus equipped with a home-built temperature-controlling device.

Results and Discussion

Analysis by SEM–EPMA

The samples were analysed by SEM simply by pouring a small amount of powder onto the sample holder, followed by gold metallisation *in vacuo* as usual. Some typical microphotographs are shown in Fig. 1. Note that, irrespective of the calcination conditions of the sample, a very high degree of sintering is present in all the micrographs. Indeed, the solid particles appear as 'glued' together by thick 'necks' of solid material. This is clearly a consequence of the high temperature of calcination. Of course, this leads to very low values of both BET surface area and porosity, the former being in any case of the order of 1 $m^2 g^{-1}$ or less and the latter of 0.05 $cm^3 g^{-1}$ or less.

The analysis by EPMA on each sample did not show any significant difference among the ratios of the various metal ions (Ca, Sr, Cu) by changing either the position or the width of the zone analysed on the sample. This ensures a good homogeneity of composition of each sample.

Analysis by XRD

The analysis by XRD always showed sharp and well resolved signals, indicating a good crystallinity of the material. The diffractograms of every couple of samples, differing only as for the procedure of calcination (*in vacuo* or in air) were

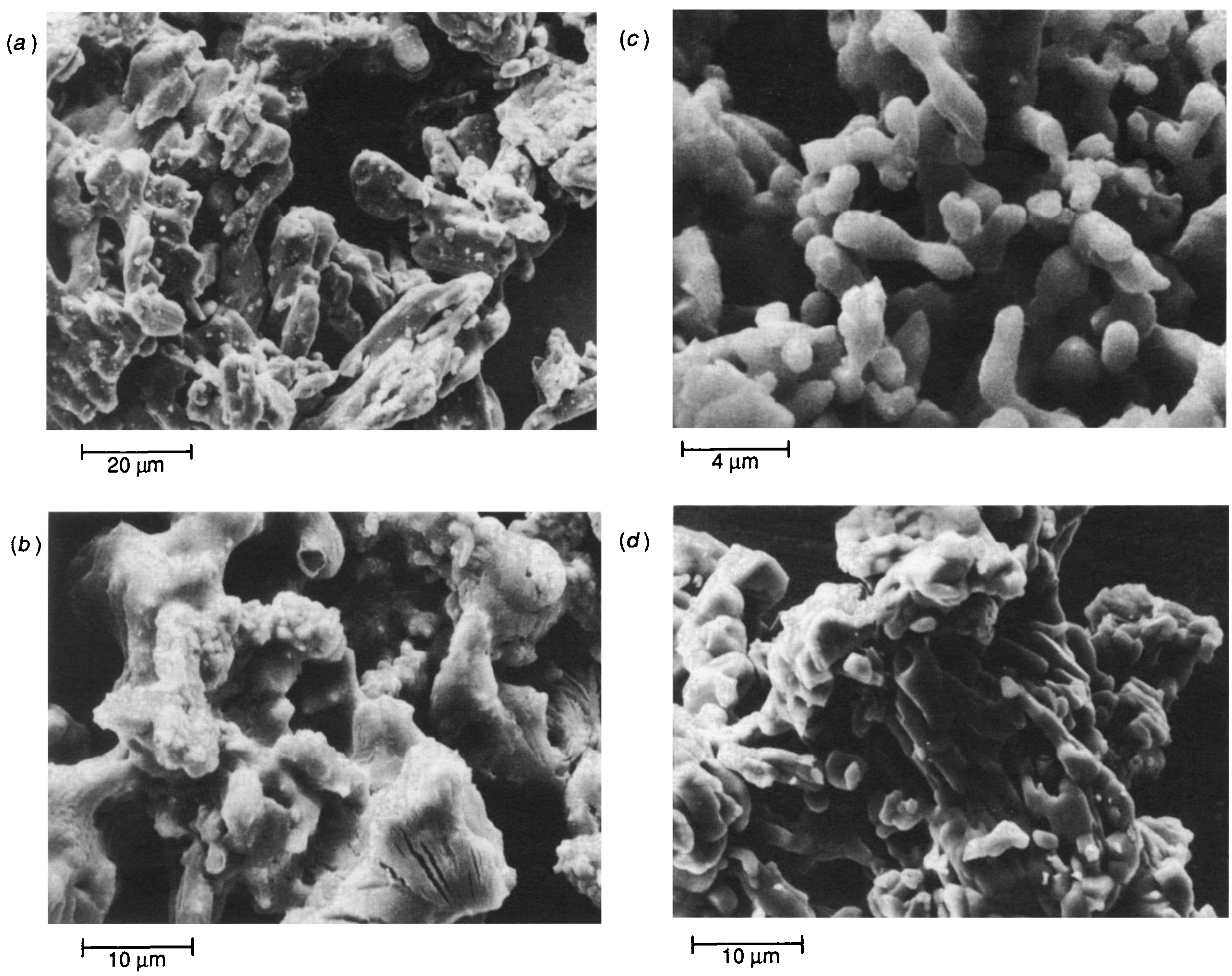

Fig. 1 Typical scanning electron micrographs of the catalysts employed: (*a*) $Sr_3Cu_5O_8$ calcined in air, (*b*) $SrCuO_2$ calcined in air, (*c*) Ca_2CuO_3 calcined *in vacuo*, (*d*) $(Ca_{0.55}Sr_{0.45})_3Cu_5O_8$ calcined in air

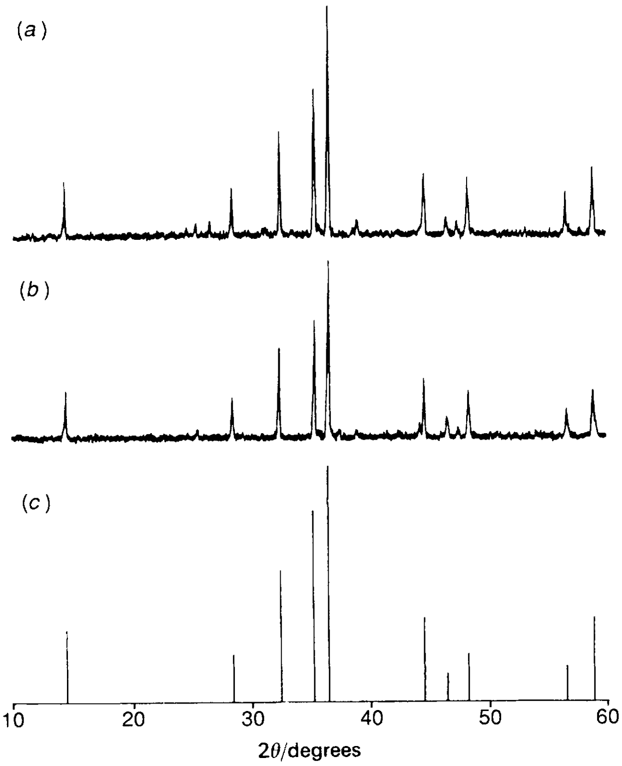

Fig. 2 X-Ray diffractogram (Debye method, Cu-Kα radiation, Ni-filtered) of the Ca_2CuO_3 catalyst, calcined (*a*) in air, (*b*) *in vacuo*, (*c*) diffractogram taken from file no. 34-0282 of ref. 13

usually perfectly identical, as shown *e.g.* in Fig. 2 for the 3_v, 3_a catalysts. The only exception was the $SrCuO_2$ catalyst, showing a distinctly different diffractogram when calcined in air [Fig. 3(*a*)] or *in vacuo* [Fig. 3(*b*)]. Additional lines are present in Fig. 3(*a*), indicating the presence of a different phase or of a polyphasic material. Comparison with the most extended collection of literature data of powder materials[13a] showed that only the Ca_2CuO_3 sample (Fig. 2) corresponds to a pattern reported in such a collection [Fig. 2(*c*)]. However, sample 1_v was found to agree completely with a pattern of $SrCuO_2$ published elsewhere[13b] and sample 4_v showed a pattern quite similar to that published for $Sr_3Cu_5O_8$.[13c]

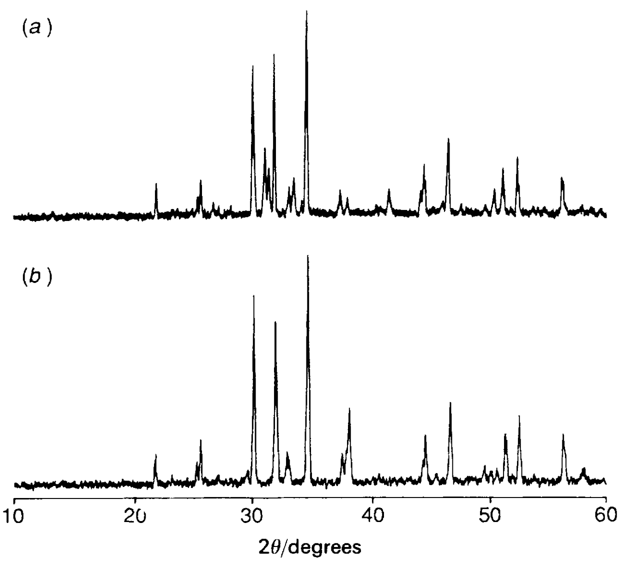

Fig. 3 X-Ray diffractogram (see Fig. 2) of the $SrCuO_2$ catalyst, calcined (*a*) in air, (*b*) *in vacuo*

Anyway, it is known that oxocuprates possess a quite complex structure, in which a considerable amount of Cu^{3+} ions are present. Among them Ca_2CuO_3, $SrCuO_2$, Sr_2CuO_3 and $SrCu_2O_2$ have received particular attention owing to their high-temperature superconductive properties.[15,16] The fundamental structure of these materials is based on corner- or edge-sharing CuO_4 square planes with Cu–O distances ranging from 1.9 to 2.04 Å. The Cu^{2+} and Cu^{3+} geometry varies, with partial distortion of the CuO_4 planes, depending both on the nature of the alkaline-earth-metal cation, M, and on the M : Cu : O ratios.

Analysis by EPR

Sample 1_v at room temperature gives an EPR pattern formed by a single 800 G broad line at $g = 2.058$ and a second 'half-field' line due to a $\Delta M_s = \pm 2$ 'forbidden' transition [Fig. 4(*a*)]. The latter is also present when the same sample (1_a) is prepared in air, while the $\Delta M_s = \pm 1$ line is displayed at a g value (2.079) higher than that for 1_v [Fig. 5(a)]. This indicates that the oxygen orbital magnetic moment contributes significantly to the energy of the unpaired $3d^9$ electron of the Cu^{2+} ions.

Furthermore, with sample 1_a the EPR line is more intense and just 600 G broad, suggesting that the interaction with oxygen also favours spin–spin exchange between unpaired electrons belonging to different Cu^{2+} ions. This is also confirmed by the fact that after a few months the EPR line narrows, probably because a small further amount of oxygen is adsorbed on the sample surface. This effect is more evident with sample 1_v than with 1_a, on which some oxygen was already present. An analogous behaviour of the spectroscopic g value is shown by $Sr_3Cu_5O_8$, the g value being slightly larger with 2_a than with 2_v (see Table 1). However, this effect is not accompanied by any narrowing of the EPR line, which in both cases is narrower than with $SrCuO_2$.

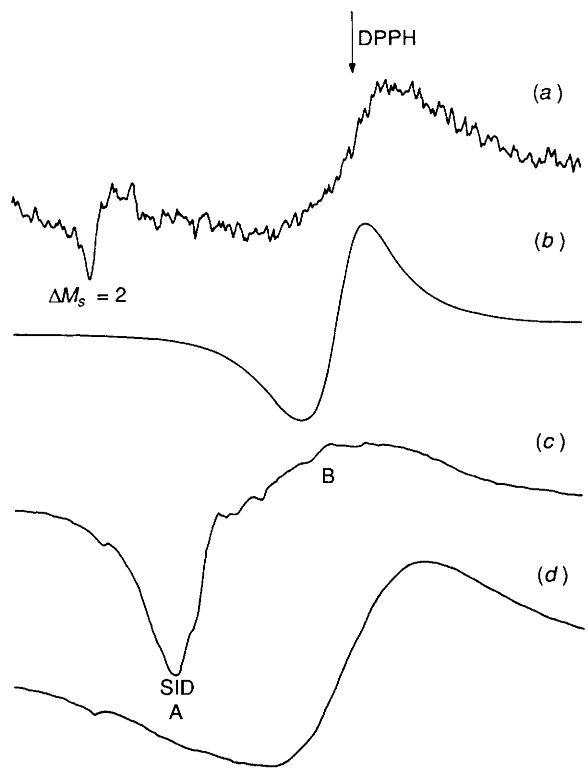

Fig. 4 Room-temperature EPR spectra of fresh samples prepared *in vacuo*: (*a*)–(*d*), samples 1_v–4_v

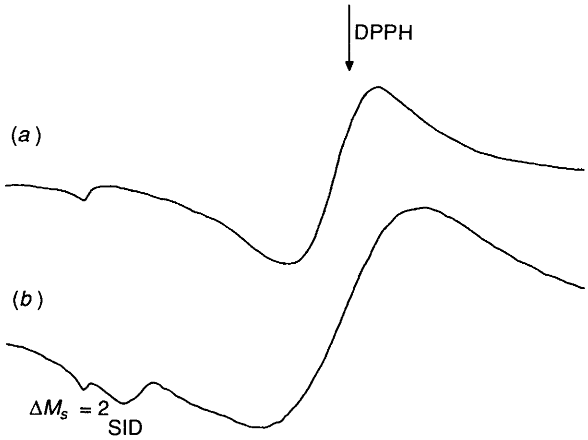

Fig. 5 Comparison between room-temperature EPR spectra of fresh (*a*) 1_a and (*b*) 4_a samples

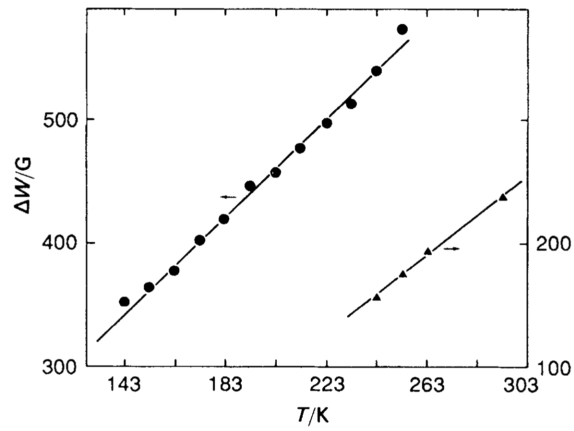

Fig. 6 EPR Lorentzian-shaped linewidth *vs.* temperature: (●) 4_v, (▲) 2_v fresh samples

2_v has been studied at temperatures down to 143 K. Line broadening was expected, but this has not been found. In fact, a narrowing of the Lorentzian-shaped line has been measured between 293 K (linewidth = 236 ± 2 G) and 243 K (linewidth = 157 ± 5 G) with a linear slope of 1.56 ± 0.08 G K^{-1} (see Fig. 6). At lower temperatures the line resolves into its different components.

When some of the Sr atoms have been substituted by Ca, forming $(Ca_{0.55}Sr_{0.45})_3Cu_5O_8$ [sample 4_v, Fig. 4(*d*)], the same unexpected line narrowing at lower temperatures is observed. However, the value of the linewidth is larger in this case, and a single Lorentzian-shaped line is always observed down to 143 K, without any resolution of the line in its components. The linewidth *vs.* temperature slope is slightly larger than with 2_v, in the present case, being 1.97 ± 0.07 G K^{-1} (see Fig. 6).

The unexpected line narrowing at low temperatures observed with 2_v and 4_v is similar to that reported for $BaCuO_2$, which displayed[17] a line (4000 G broad at 180 K), rapidly narrowing with decreasing temperature, and reaching less than 600 G at 14 K (with slope 24 G K^{-1}). Similar effects had been previously reported for single crystals of CuX_4^{2-} (X = Cl, Br) salts based on ferromagnetic layers of S = 1/2 Cu^{2+} sites.[18–20] In ref. 20 a review of the literature data is also reported. Slopes $b = d\,\Delta H/dT$ ranging between 0.240 and 0.109 for chloride salts and between 1.45 and 2.10 for bromide salts have been reported there. The results obtained by us with 2_v and 4_v agree with the literature data falling in the second range. To the best of our knowledge, the first example[21,22] of EPR linewidth broadening of this type is for $Cu(HCO_2)_2 \cdot 4H_2O$. This compound possesses a crystal structure having large superexchange interactions (antiferromagnets) as well as sufficiently low symmetry. As a consequence, the antisymmetric exchange interaction is known to account for the weak ferromagnetism. So the layer-like crystal closely approximates a two-dimensional antiferromagnet with strong superexchange between Cu^{2+} ions belonging to the same layers. The linear temperature dependence was then accounted for by the phonon modulation of the antisymmetric exchange interaction, through single-phonon absorption and emission processes involving spin flips. To the best of our knowledge, no other technique is so specific for detecting this kind of layer-like structure, provided of course that the sample is not EPR-silent.

Table 1 *g* value and linewidth of single EPR lines

ref.	sample	*g*/G	linewidth/G
1_v	$SrCuO_2$	2.058	800
1_a		2.079	600
2_v	$Sr_3Cu_5O_8$	2.064	420
2_a		2.073	420
4_v	$(Ca_{0.55}Sr_{0.45})_3Cu_5O_8$	2.070	1030
4_a		2.070	1030

3_v and 3_a samples are not reported owing to their completely different spectrum (see text).

This effect can no longer be observed in air. In fact a low-field line, perhaps already present with very low intensity with 4_v, becomes intense with 4_a at *ca.* 2060 G [see Fig. 5(*b*)], indicating that in this case strong dipolar interactions occur between the unpaired electrons of neighbouring Cu^{2+} ions (*vide infra*) contrasting the long-range effect of phonon modulation of the antisymmetric exchange interactions.

The EPR spectra obtained with 3_a and 3_v are composed of two independent patterns [Fig. 4(*c*)]. The main feature (A) is a broad asymmetric line. Its peak is at *ca.* 2130 G at room temperature. At the same temperature this line is observed at magnetic field values slightly lower (2100 G) when the sample has been prepared in air (3_a). In both cases a second EPR pattern [B, Fig. 4(*c*)] is superimposed, formed by more lines less intense than A and centred at higher fields. They can probably be attributed to weakly interacting dipoles forming a triplet state.[23]

A appears at room temperature between 1900 and 2400 G with Ca_2CuO_3 both *in vacuo* (3_v) and in air (3_a) as well as with $(Ca_{0.55}Sr_{0.45})_3Cu_5O_8$, but just in air ($4_a$). This line is similar to that reported in the literature for the triplet state of dimeric copper complexes of 2,2′-dipyridyl (Cu–Cu distance ranging between 2.85 Å and 2.89 Å),[24] for potassium tricyanocuprate(II)[25] and for other cluster compounds of the general type $(Cu_4OX_{10-n}L_n)^{n-4}$ (Cu–Cu average distance 3.13 Å) where X represents a chloride or bromide ion and L represents a Lewis base ligand.[26] This is not surprising, as the distance between two neighbouring Cu^{2+} ions in Ca_2CuO_3 is just 3.25 Å.[15,16] In the above literature cases it has been shown that the formation of particularly strongly interacting electron dipoles (SID) accounts for such a peculiar EPR line at low field, owing to the formation of the copper dimers or clusters 'bridged' by oxygen atoms or by other ligands.[27]

Catalytic Activity by Pulse-reactor and TPD–TPR Techniques

Oxidation of Toluene

The catalytic behaviour of the present oxide mixtures was analysed only through pulse-reactor experiments. The first reaction considered was the mild oxidation of toluene. The runs were carried out in every case on *ca.* 300 mg of catalyst, through which a continuous flow (15 cm^3 min^{-1}) of helium was drawn as carrier gas. The pulses of reactant(s) were performed either at relatively low (373 K) or at high temperature (673 K). In any case, the most significant mass fragments were simultaneously monitored during the whole experiment, in order to detect the species outcoming from the reactor. The a.m.u. values, characteristic of the various species, were chosen[28,29] as: 18 (H_2O), 30 (CO), 32 (O_2), 44 (CO_2), 92 (toluene) and 106 (benzaldehyde). In spite of the low intensity (0.2% of the a.m.u. = 28 parent peak) of the a.m.u. = 30 fragment of CO, we preferred to monitor CO through the latter a.m.u. value, since the a.m.u. = 28, which is common to molecular nitrogen, is usually affected by a high background value.

A series of TPD runs were carried out by injecting 0.5 mm^3 pulses of toluene during an initial 373 K isotherm, followed by a 20 K min^{-1} TPD ramp up to a final 823 K isotherm. Excluding the 4_v and 4_a samples, all the other catalysts proved unable to adsorb significant amounts of toluene. As a consequence, only the 4_v and 4_a samples showed some catalytic activity for toluene oxidation. The most interesting results were obtained with the 4_v catalyst. An example of the spectra monitored during a typical 373 K isothermal experiment is shown in Fig. 7. During these runs usually two 0.5 mm^3 pulses of toluene were injected, followed by three 1 cm^3 pulses of air and finally by a simultaneous injection of the two reactants. The formation of benzaldehyde (a.m.u. = 106) was observed in correspondence with each pulse of toluene, that of CO, CO_2 and H_2O (a.m.u. = 30, 44 and 18, respectively) in correspondence with each of the pulses, of either pure toluene, pure air, or both the reactants simultaneously.

The most important observations relative to oxidation of toluene over the 4_v catalyst may be summarised as follows: (i) The formation of the aldehyde on the fresh catalyst (first two pulses of pure toluene) must be due to relatively free active oxygen species present in the solid, since no pulses of such a gas were injected on the fresh sample. (ii) At least a part of the toluene is adsorbed onto sites unable to activate it for the desired reaction. Indeed, this part of the toluene is desorbed unaltered by further pulses of oxygen (see the three air pulses), without the formation of new aldehyde. (iii) A further part of the toluene is completely oxidised to CO, CO_2 and H_2O, probably after being adsorbed on higher-energy sites, provided a sufficient amount of active oxygen is present on the catalyst.

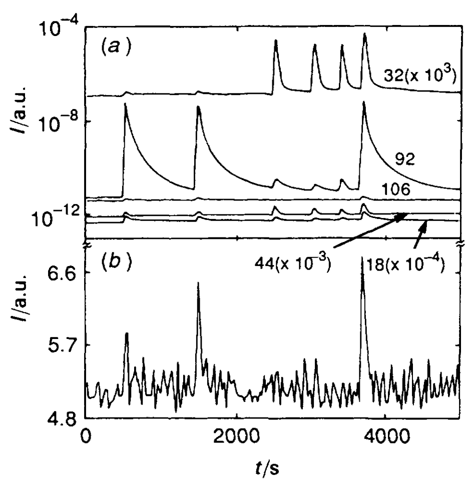

Fig. 7 Toluene oxidation tests. (*a*) Typical example of pulse-reaction over 4_v catalyst. From left: 2 × 0.5 mm^3 pulses of toluene, 3 × 1 cm^3 pulses of air, simultaneous 1 × 0.5 mm^3 + 1 cm^3 pulses of toluene and air, respectively. Catalyst weight, 288 mg. Carrier gas (He) flow rate: 20 cm^3 min^{-1}. Figures indicate the a.m.u. value of the signal. The reducing or multiplying factor is given in parentheses. (*b*) Enlargement of the a.m.u. = 106 (benzaldehyde) signal

Decomposition of NO

More interesting results were obtained when employing our catalysts for the decomposition of NO to $N_2 + O_2$. These runs were carried out by the same pulse-reactor assembly, usually by injecting a series of seven 1 cm^3 pulses of a pre-formed 100 ppm NO in N_2 gas mixture, *i.e.* a mixture mimicking the composition of the exhaust gas from power-station gas burners. The characteristic a.m.u. values monitored for the various species were chosen[28,29] as: 30 (NO), 32 (O_2) and 46 (NO_2). It was not possible to monitor N_2O, owing to the simultaneous presence of the very large excess of N_2, the fragmentation of which gives practically the same a.m.u. values as N_2O.

Data were collected by varying the temperature of the initial isotherm, preceding the TPD ramp, from 333 to 373 K and then up to 673 K in 100 K steps. The TPD ramp (10 K min^{-1}) was always carried out up to the final 20 min isotherm at 823 K. The catalysts tested were 1_v–4_v and 3_a.

$(Ca_{0.55}Sr_{0.45})_3Cu_5O_8$ *Catalyst*

The first series of runs, concerning the 4_v catalyst, showed that the formation of O_2, denoting the decomposition of NO, took place at relatively low temperature ($\leqslant$373 K) (Fig. 8) and that a considerable amount of NO remained adsorbed at such low temperatures [Fig. 8(*c*)]. At higher temperatures (473 K), no decomposition of NO was detected (Fig. 9) the a.m.u. = 32 signal, corresponding to oxygen, remaining completely flat [Fig. 9(*b*)]. At further higher temperature (573 K) the catalyst remained unactive (Fig. 10), with some NO still remaining adsorbed on it [Fig. 10(*c*)]. No formation of NO_2 was ever detected at any reaction temperature. These rather strange phenomena led us to a more detailed study of the interaction of NO with all the present catalysts. The results will soon be reported elsewhere.[30]

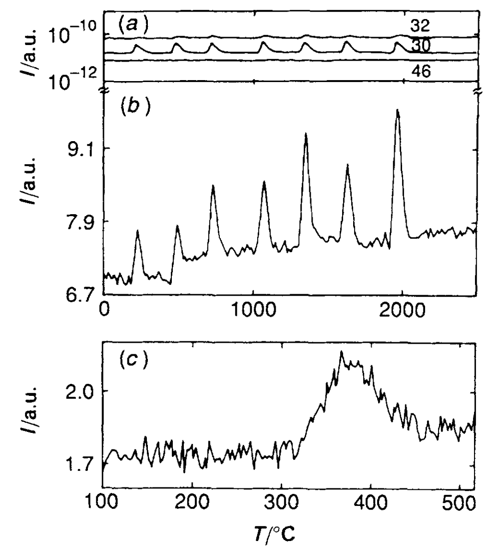

Fig. 8 NO decomposition tests. (*a*) Typical example of pulse-reaction over 4_v catalyst. Seven 1 cm^3 pulses of 100 ppm NO in N_2 gas mixture. Catalyst weight, 236 mg. Carrier gas (He) flow rate, 20 cm^3 min^{-1}. *T* = 373 K. Figures on the lines indicate the a.m.u. value. (*b*) Enlargement of the a.m.u. = 32 (oxygen) signal. (*c*) TPD of adsorbed NO after the sequence of pulses of Fig. 8(*a*). Temperature ramp, 20 K min^{-1} up to the final 823 K isotherm

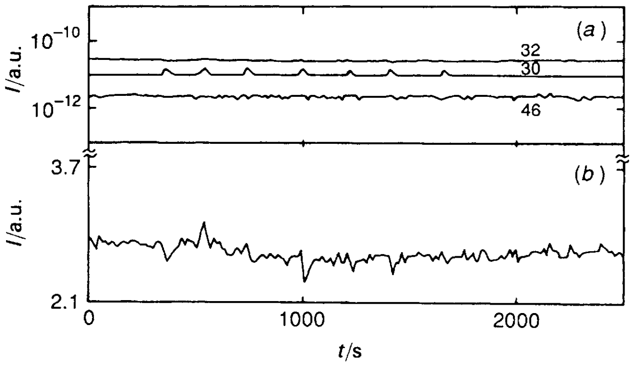

Fig. 9 NO decomposition tests. (*a*) As for Fig. 8(*a*), $T = 473$ K. (*b*) Enlargement of the a.m.u. = 32 (oxygen) signal

$SrCuO_2$ *Catalyst*

All the runs carried out as previously described on 1_v and 1_a at any temperature showed no adsorption of NO and the complete inactivity of this catalyst for the present reaction.

$Sr_3Cu_5O_8$ *Catalyst*

With 2_v the activity for the NO decomposition was quite high for reaction temperatures up to 573 K, going through a maximum at 473 K (Fig. 11). Note that the fresh catalyst is always extremely active, although the activity declines with increasing the number of pulses [see *e.g.* Fig. 11(*b*)]. Furthermore, as for all the active catalysts, a substantial amount of NO is adsorbed onto the catalyst surface, up to the highest temperature (573 K) at which activity is still displayed, and it is desorbed during the subsequent usual TPD ramp (Fig. 12). It was also noticed that the desorption of oxygen takes place at a much higher temperature with respect to desorption of NO.

Ca_2CuO_3 *Catalyst*

This catalyst displayed a considerably different behaviour compared with the other catalysts. With both 3_v and 3_a only a modest activity at $T \leqslant 473$ K was noted, rapidly declining with increasing number of NO pulses. The activity went through a maximum at $T = 373$ K and again a burst of

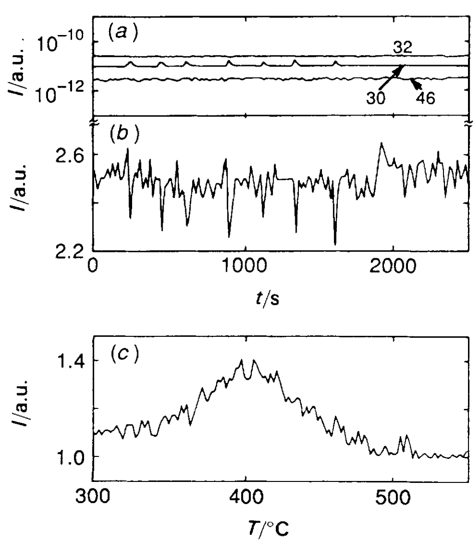

Fig. 10 NO decomposition tests. (*a*) As for Fig. 8(*a*), $T = 573$ K. (*b*) Enlargement of the a.m.u. = 32 (oxygen) signal. (*c*) TPD of the adsorbed NO after the sequence of pulses of (*a*)

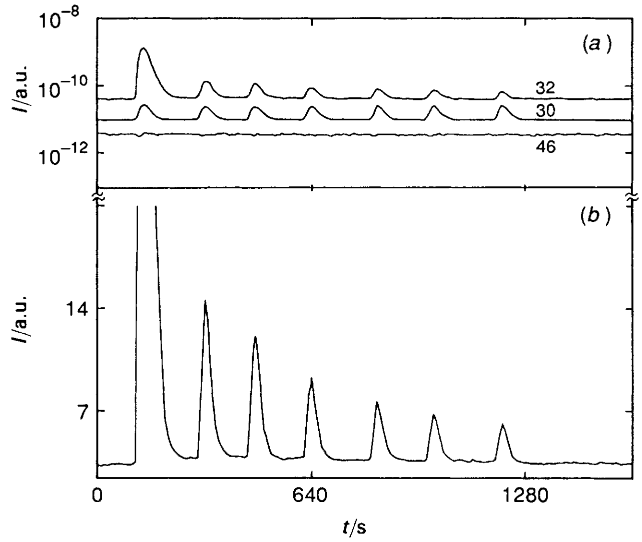

Fig. 11 NO decomposition tests. (*a*) Typical example of pulse-reaction over 2_v catalyst. Reaction conditions as for Fig. 8(*a*). $T = 473$ K. Catalyst weight, 343 mg. (*b*) Enlargement of the a.m.u. = 32 (oxygen) signal

oxygen on the fresh catalyst was noticed corresponding with the first NO pulse. A typical example is shown in Fig. 13.

However, during the TPD runs following every series of NO pulses, no desorption of NO, or of O_2, was ever detected, whereas a considerable amount of NO_2 was desorbed at quite high temperature (see *e.g.*, Fig. 14).

Correlation between Catalyst Activity and EPR-revealed Structure

Samples 1 and 3 are poor catalysts for both the decomposition of NO and the oxidation of toluene. When these samples have been calcined in air, their EPR signals are narrower [see Fig. 5(*a*) for 1_a], indicating that oxygen favours a faster electron spin–spin exchange between different Cu^{2+} ions. A similar linewidth narrowing effect is observed with the same samples after the reactions. In contrast, both samples 2 and 4 proved to be active and selective catalysts for the dissociation of NO, the latter being more durable than the former, and also catalysing the oxidation of toluene. These two samples are the only ones possessing a layer-like crystal structure which approximates a two-dimensional antiferromagnet, as revealed by their EPR linewidth dependence on temperature.[18,20,22]

Hence, the catalytic activity seems connected with this kind of crystal structure. This is confirmed by the fact that sample 4, which is the best catalyst, is also the only one maintaining the layer-like structure over the whole range of measured

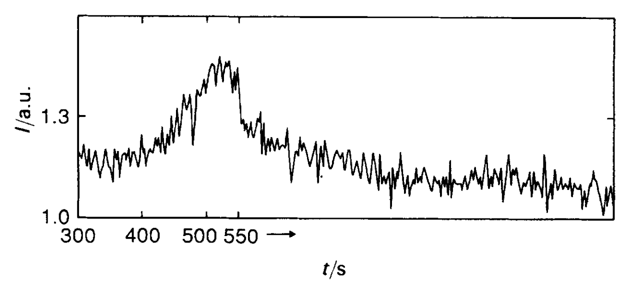

Fig. 12 NO decomposition tests. TPD of the adsorbed NO from 2_v catalyst pretreated as for Fig. 11, but at 573 K

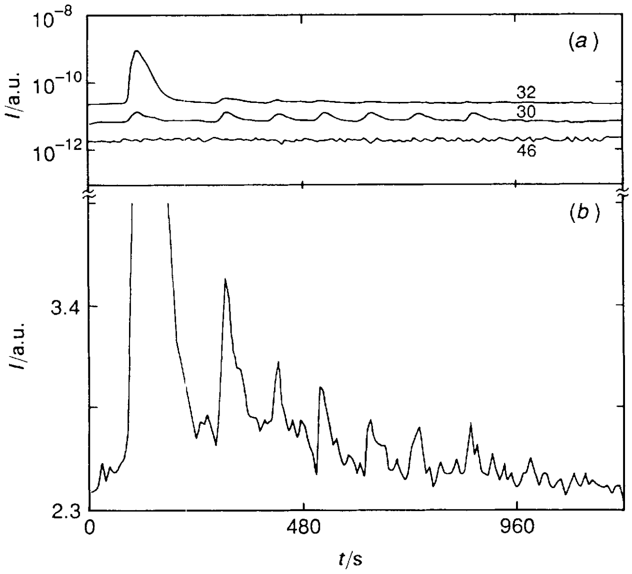

Fig. 13 (*a*) NO decomposition tests. Typical example of pulse-reaction over 3_v. Reaction conditions as for Fig. 8(*a*). $T = 373$ K, catalyst weight, 276 mg. (*b*) Enlargement of the a.m.u. = 32 (oxygen) signal

temperatures (143–333 K), while sample 2, which is less good as a catalyst, does not show that kind of crystal structure at temperatures lower than 243 K.

Another important difference must be outlined between the EPR spectra of these two samples. Oxygen, present during the toluene oxidation or coming from the NO decomposition, narrows the line shape of 2_v as also happens with 2_a in air. At variance, oxygen changes significantly the EPR pattern of sample 4, by introducing a SID (low-field) EPR line [see Fig. 15(*a*) and (*b*)] similar to that observed with the same sample calcined in air [Fig. 5(*b*)]. This means that the oxygen present during toluene oxidation or coming from NO decomposition bridges together Cu^{2+} neighbouring ions forming SID systems. The latter are held together by oxygen atoms adsorbed onto the catalyst. As a further consequence, those exchange phenomena, affecting 1_a and 3_a fresh samples or 1_v and 3_v after reaction, are not observed with 4_a or 4_v after reaction.

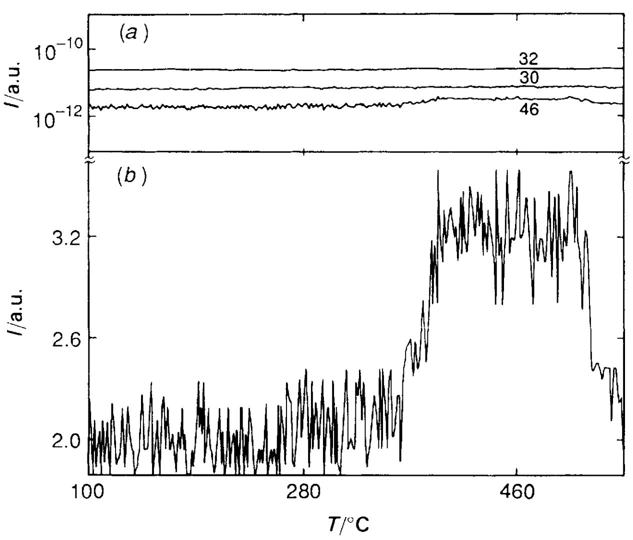

Fig. 14 NO decomposition tests. (*a*) TPD of NO, O_2 and NO_2 from 3_v catalyst after the pretreatment of Fig. 13. (*b*) Enlargement of the a.m.u. = 46 (NO_2) signal

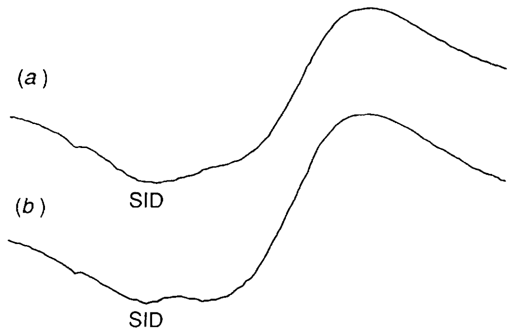

Fig. 15 EPR spectra of 4_v catalyst after (*a*) toluene oxidation, (*b*) NO decomposition

Finally, we must also outline that, in contrast, the adsorption of oxygen through the formation of copper dimers or clusters cannot happen with samples like 3. Indeed, in these solids almost all of the Cu^{2+} ions are already linked to oxygen atoms,[15,16] even before the reaction, and a great concentration of SID systems is therefore observed even with fresh samples prepared *in vacuo* [A, Fig. 4(*c*)]. No further dimeric copper species can be formed in this case, and the reactions here examined cannot be catalysed through this mechanism.

References

1 R. K. Grasselli and J. D. Burrington, in *Adv. Catal.* ed. D. D. Eley, H. Pines and P. B. Weisz, Academic Press, New York, 1981, vol. 30, p. 133.
2 K. K. Wu, J. R. Ashburn, C. G. Torng, P. H. Hor, R. L. Meng, L. Gao, Z. J. Huang, Y. Q. Wang and C. W. Chu, *Phys. Rev. Lett.*, 1987, **58**, 908.
3 R. J. Cava, B. Batlogg, R. B. van Dover, D. W. Murphy, S. Sunshine, T. Siegrist, J. P. Remeika, E. A. Reitmann, S. Zahurak and G. Espinosa, *Phys. Rev. Lett.*, 1987, **58**, 1676.
4 W. E. Farneth, R. K. Bordia, E. M. McCarron, M. K. Crawford and R. B. Flippen, *Solid State Commun.*, 1988, **66**, 953.
5 D. Klissurski, J. Pesheva, Y. Dimitriev, N. Abatieva and L. Minchev, in *New Developments in Selective Oxidation*, ed. G. Centi and F. Trifirò, Preprints, Univ. Bologna, 1989, paper F31.
6 J. Otamiri, A. Andersson, S. Hansen and J. O. Bovin, in *New Developments in Selective Oxidation*, ed. G. Centi and F. Trifirò, Preprints, Univ. Bologna, 1989, Paper E4.
7 S. Hansen, J. Otamiri, J-O. Bovin and A. Andersson, *Nature*, 1988, **334**, 143.
8 (*a*) B. A. Lur'e, V. V. Seregin, A. N. Savin and B. B. Svetlov, *Russ. J. Phys. Chem.*, 1984, **58**, 231; (*b*) K. Tabata, *J. Mater. Sci. Lett.*, 1988, **7**, 147; (*c*) K. Tabata and M. Misono, *Catal. Today*, 1990, **8**, 249.
9 A. Manthiram, J. S. Swinnea, Z. T. Sui, H. Steinfink and J. B. Goodenough, *J. Am. Chem. Soc.*, 1987, **109**, 6667.
10 M. O'Keeffe and S. Hansen, *J. Am. Chem. Soc.*, 1988, **110**, 1506.
11 J. Haber, in *Surface Properties and Catalysis by Non-Metals*, ed. J. P. Bonnelle, B. Delmon and E. Derouane, Reidel Dordrecht, 1983, p. 1.
12 R. K. Grasselli, J. F. Brazdil and J. D. Burrington, *Proc. 8th Int. Cong. Catal.*, Verlag Chemie, Weinheim, 1984, vol. V, p. 369.
13 (*a*) *Selected Powder Diffraction Data*, JCPDS, Swarthmore, PA, 1974, DBM/1/23 and PD 15-39 i.RB; (*b*) V. D. Zhuravlev, Yu. A. Velikodnyi and L. V. Kristallov, *Russ. J. Inorg. Chem.*, 1987, **32**, 3060; (*c*) J. Liang and Z. Chen, *XV Congr. Intern. Union Cryst.*, Coll. Abstr., France, July 1990, p. C336.
14 L. Forni, M. Toscano and P. Pollesel, *J. Catal.*, 1991, **130**, 392.
15 Von Chr. L. Teske and H. Müller-Buschbaum, *Zeit. Anorg. Allgem. Chem.*, 1969, **370**, 134; 1969, **371**, 325; 1970, **379**, 113; 1970, **379**, 234.
16 M. T. Weller and D. R. Lines, *J. Solid State Chem.*, 1989, **82**, 21.
17 J. Genossar, D. Shaltiel, V. Zevin, A. Grayevsky and B. Fisher, *J. Phys. Condens. Matter I*, 1989, 9471.
18 J. E. Drumheller, D. H. Dickey, R. P. Reklis and C. E. Zaspel, *Phys. Rev. B*, 1972, **5**, 4631.
19 Z. S. Soos, K. T. McGregor, T. T. P. Cheung and A. J. Silverstein, *Phys. Rev. B*, 1977, **16**, 3036.
20 R. D. Willet and R. J. Wong, *J. Mag. Reson.*, 1981, **42**, 446.

21 M. S. Seehra and T. G. Castner Jr., *Phys. Kondens. Mater.*, 1968, **7**, 185.
22 T. G. Castner Jr. and M. S. Seehra, *Phys. Rev. B*, 1971, **4**, 38.
23 E. Wasserman, L. C. Snyder and W. A. Yager, *J. Chem. Phys.*, 1964, **41**, 1763.
24 J. A. Barnes, D. J. Hodgson and W. E. Hatfield, *Inorg. Chem.*, 1972, **11**, 144.
25 J. Kohout, M. Liska and M. Hvastijova', *Inorg. Chim. Acta*, 1977, **25**, L71.
26 R. C. Dickinson, F. T. Helm, W. A. Baker Jr., T. D. Black and W. H. Watson Jr., *Inorg. Chem.*, 1977, **16**, 1530.
27 J. R. Wasson, C. I. Shyr and C. Trapp, *Inorg. Chem.*, 1968, **7**, 469.
28 S. R. Heller and G. W. A. Milne, *EPA-NIH Mass Spectral Data Base*, National Bureau of Standards, U.S. Government Printing Office, Washington D.C., 1978, vol. 1, 5.
29 R. D. Craig and E. H. Harden, *Vacuum*, 1966, **16**, 67.
30 L. Forni, F. P. Vatti, C. Oliva, N. A. Sinitsina, A. V. Moev and A. V. Vishniakov, *Russ. J. Phys. Chem.*, submitted.

Paper 1/05294B; *Received* 18*th October*, 1991